Mechanical properties of striped bass fish skin: Evidence of an exotendon function of the stratum compactum

Lawrence Szewciw, Francois Barthelat*

Department of Mechanical Engineering, McGill University, Macdonald Engineering Building, 817 Sherbrooke St. West, Montreal, Quebec, Canada H3A 0C3

ABSTRACT

Teleost fish skin is a multifunctional natural material with high penetration resistance owing to specialized puncture mechanisms of both the individual scale and the intact scaled integument. In this paper, we explore the possible additional role of the skin in fish undulatory locomotion by examining the structural and mechanical properties of the dermal stratum (s.) compactum layer of striped bass (*Morone saxatilis*) skin. The structure, mechanical response and function of s. compactum was investigated by combining several methods: optical microscopy and histology, tensile tests on descaled skin specimens in different anatomical locations and orientations, puncture tests, and flexural tests on whole fish with disruption of the s. compactum. Local histological features of the s. compactum, such as collagen fiber angle and degree of crimping, were shown to explain corresponding patterns determined for the tensile properties of the skin along the long axis of the fish, including changes in stiffness, strength and locking strain at stiffening. The fish bending tests demonstrated a tendon-like response of the whole fish and a significant contribution of the s. compactum to the flexural stiffness of the fish. Collectively, the findings show that the s. compactum is a strong tissue with a tendon-like nonlinear response, and which provides an appreciable mechanical protection against sharp puncture and lacerations. Our results also support the theory of an exotendon function of the s. compactum in teleost fish skin. These findings may inspire the design of new multifunctional protective and locomotory systems for a variety of engineering applications.
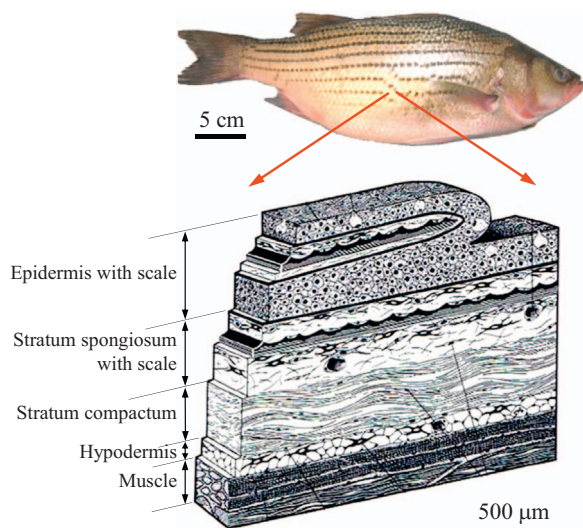
1. Introduction

The scaled skin of striped bass (*Morone saxatilis*), a common teleost fish, is a natural material with high protective capacity. Specialized mechanisms evolved by the skin were recently revealed at different length scales by investigating puncture mechanisms at both the level of the individual fish scale (Zhu et al., 2012) and at the tissue level where the mechanical interaction of overlapping scales contributes to the puncture resistance of the skin (Zhu et al., 2013). Individual scales have a high resistance to sharp penetration because of their layered structure and controlled failure mechanisms (Zhu et al., 2012; Bruet et al., 2008; Meyers et al., 2012; Yang et al., 2013). The outer layer of the scale, made of partially mineralized collagen fibrils, fails in a highly controlled fashion in the case of sharp puncture. The inner layer of the scale, made of a dense crossply of collagen fibrils, acts as a membrane which limits local deflection and absorbs mechanical energy (Zhu et al., 2012). The inner collagen layer of the scales is amongst the toughest collagenous tissues known (Dastjerdi and Barthelat, 2015). Overlapping scales act collectively, and their mechan-ical interactions distribute the puncture over large areas, limiting local deflections (Vernerey and Barthelat, 2010) and protecting the softer and more fragile underlying tissues against blunt trauma (Zhu et al., 2013).

In addition to delaying damage from sharp puncture, the interac-tions between the scales may also play an important role in fish undulatory locomotion during which the scales may interact on the inner, concave side of the fish at the end of a swimming stroke and at a high body curvature. In this scenario, the scales interlock and store elastic strain energy at the end of each stroke, which can be released to initiate and rapidly accelerate the next stroke. The scales would therefore function as an external tendon (or exotendon) to enhance swimming efficiency (reduce the energy required for locomotion via facilitation of muscle contraction) as observed in gar fish (Long et al., 1996). However, the lower layer of the dermis, the collagenous stratum (s.) compactum (Fig. 1), has received the most attention as a potential energy storage device providing an exotendon function to the skin of fish and sharks (Long et al., 1996; Wainwright et al., 1978; Whitear, 1986; Naresh et al., 1997; Elliot, 2000; Hebrank and Hebrank, 1986).

* Corresponding author.
  E-mail addresses: lawrence.szewciw@mail.mcgill.ca (L. Szewciw), francois.barthelat@mcgill.ca (F. Barthelat).
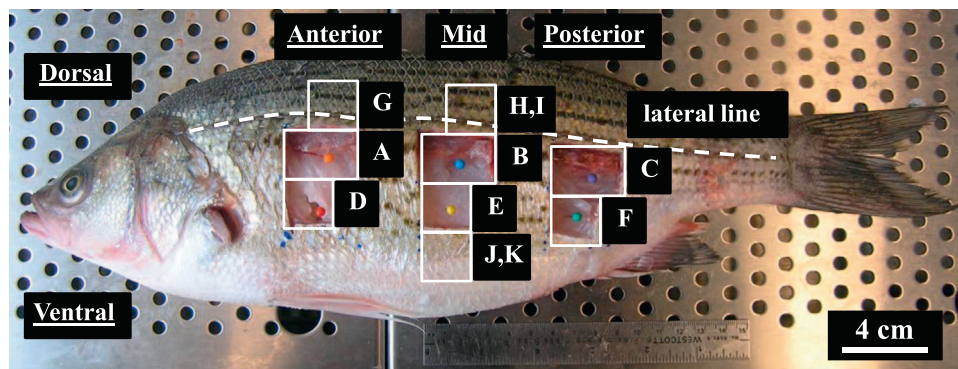
Fig. 1. Generalized cross section of teleost fish skin showing: the cuticle and epidermis, dermal scales with upper mineralized and lower unmineralized layers, the gelatinous s. spongiosum that surrounds the scales, the s. compactum consisting of a cross-helical arrangement of collagen fibers winding about the axis of the fish, and the underlying hypodermis and muscle (adapted from (Elliot, 2000)).

The general structure of the s. compactum was first described by Motta (1977) for sharks. It consists of a cross-helical arrangement of collagen fibers whose fiber angles relative to the long axis of the fish vary along its anteroposterior (A-P) length, and whose alternating lamellae of left- and right helically-wound fibers were later shown to exhibit varying degrees of crimping or waviness along the fiber axis (Naresh et al., 1997) (Fig. 1). Shortly thereafter, Wainwright et al., (1978) were the first to propose that the s. compactum acts as a whole body tendon in sharks. Wainwright et al. (1978) based their hypothesis on mechanical theory described in (Wainwright et al., 1976) on open- and closed fiber-reinforced cylinders (with helically-wound fibers similar to the s. compactum). This model explained how the volume of the cylinder changes under tension or compression, as a function of change in fiber angle. This model also predicted that a fiber angle of 54° was the most adapted to resist principal stresses arising from pressurizing the cylinder. Interestingly, this optimal angle is close to the actual angles of the stratum compactum fibers wound around the body of sharks and fish (Wainwright et al., 1978; Naresh et al., 1997; Hebrank and Hebrank, 1986; Motta, 1977; Wainwright et al., 1976). Given a cylinder wound with fibers of fixed length, this particular angle also generates the highest volume for the cylinder for given axial deformations (Wainwright et al., 1976). Wainwright et al. (1978) applied this fiber-wound cylinder theory to the s. compactum of lemon sharks (*Negaprion brevirostris*) in order to explain the proposed exotendon

function and how the s. compactum behaves under bending deformation during locomotion, but the precise operation of the s. compactum during swimming (or its exotendon mechanism) is still not completely understood.

Subsequently, Hebrank and Hebrank (1986) studied the possible exotendon function of the s. compactum in two species of teleost fish (Norfolk spot, *Leiostomus xanthurus* and skipjack tuna, *Katsuwonus pelamis*) as opposed to sharks. By examining the structure of the skin including collagen fiber angles of the s. compactum and by performing uniaxial and biaxial tensile tests on the skin, Hebrank and Hebrank (1986) suggested that s. compactum does not play a tendon role in teleosts, but their evidence of a lack of tendon function was inconclusive. Naresh et al. (1997) revealed that the s. compactum of their model shark species (spadenose shark, *Carcharias laticaudus*), similar to the sharks and teleosts studied in Wainwright et al. (1978), Hebrank and Hebrank and Hebrank (1986) and Motta (1977), displayed a pattern of decreased collagen fiber angle towards the caudal end of the shark, and also a pattern of decreased crimping or waviness of collagen fibers towards the tail end. The elastin content of the s. compactum was also examined as an additional variable contributing to the differing properties of the skin along the A-P axis, with the anterior region containing a higher proportion of elastin. By performing tensile tests on specimens in different directions ("parallel" or along the A-P axis, "perpendicular" or along the dorsoventral D-V axis, and AV-PD and AD-PV "diagonal" orientations), the mechanical properties of the skin from the different A-P regions of the shark were explained in terms of its structure and more specifically by the collagen fiber and crimp angles, and the elastin content of the s. compactum. The histology results and mechanical properties of the s. compactum reported by Naresh et al. (1997) for *C. laticaudus* shark skin were consistent with the original exotendon hypothesis proposed by Wainwright et al. (1978) for the s. compactum of *N. brevirostris* shark skin.

A comprehensive examination of the structure, mechanical responses under tension, flexure and puncture, and functions of the s. compactum of a teleost fish has yet to be provided in the literature. In this study, we provide a characterization of the structural and mechanical properties of the s. compactum from the common teleost fish, striped bass (*M. saxatilis*). We report histological data (collagen fiber and crimp angles) in addition to tensile data for the s. compactum of this teleost fish. We also report bending tests on whole descaled fish and descaled fish where the structure of the s. compactum was severely disrupted with laceration, to experimentally assess its mechanical contribution to bending and thus further explore the s. compactum exotendon hypothesis for striped bass fish skin.

Fig. 2. Location of striped bass skin samples collected for measurement of collagen fiber & crimp angles of the s. compactum layer. Samples were dissected at three locations along the anteroposterior (A-P) axis (anterior, mid & posterior locations), and at different distances away from the lateral line along the dorsoventral (D-V) axis. Samples A-C were used to produce sagittal sections, whereas samples D-K were used to produce transverse sections along the D-V axis.

2. Microstructure of the s. compactum
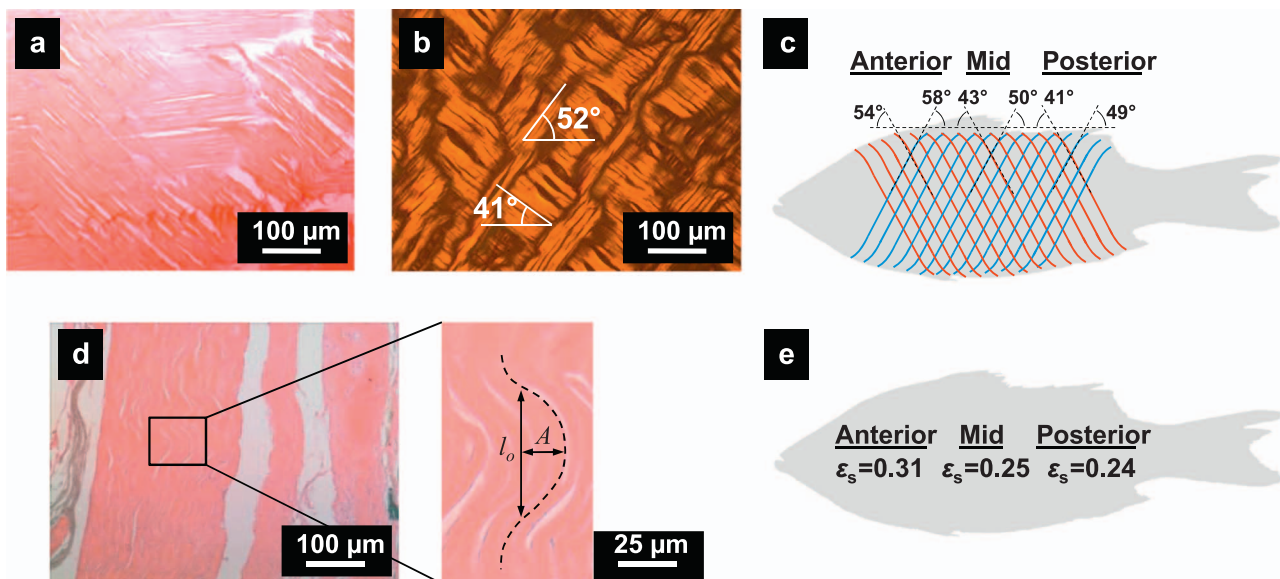
2.1. Experimental setup

The histology methods used to characterize the structure of the s. compactum were similar to those followed by Naresh et al. (1997). Whole, fresh (recently deceased and on ice) striped bass (*Morone saxatilis*) fish were acquired from a local fish store (Montreal, QC, Canada) and originated from the fish supplier, Nature's Catch Inc., Clarksdale, MS, USA. The fish had a length (l) and width (w) of about (~) 40 cm and 10 cm, respectively, and were kept on ice before sample collection. Tissue sample collection commenced within a few hours of purchasing the fish and tissue samples were dissected from three fish. One fish was fully descaled on its left side from the lateral line down to the ventrum. Using a scalpel, three tissue blocks (samples A-C in Fig. 2) were dissected from the fish immediately ventral to the lateral line and at three anteroposterior (A-P) locations (anterior, mid and posterior). The dimensions of the tissue blocks were, l (A-P axis)×w (D-V axis)×depth d=3 cm×2 cm×0.5 mm. Each tissue block was immersed in 100 ml of 10% neutral buffered formalin (NBF) for tissue fixation. Three additional, smaller tissue blocks (samples D-F in Fig. 2) were dissected from the fish immediately ventral to the first three samples. The dimensions of the smaller tissue blocks were, l ×w×d=2 cm×1.5 cm×0.5 mm. The mean and standard error (s.e.) for the thickness of samples A-F (n=6) were $0.467 \pm 3.07 \cdot 10^{-2}$ mm and measured using digital calipers. Each of the smaller tissue blocks was immersed in 50 ml of 10% NBF. From the other two fish, five similar samples were prepared in 10% NBF, and were dissected from the anterior and mid regions of the fish. The anterior specimen (G) was located directly above the lateral line, and the four mid specimens (H, I and J, K) were located directly above the lateral line and close to the ventrum, respectively (Fig. 2). The five extra specimens (G-K) were immersed in 50 ml of 10% NBF. The tissue samples were stored at 4 °C and submitted for histological processing.

The tissue blocks were dehydrated in ethanol, embedded in paraffin, and sectioned into either ~5 µm sagittal (horizontal) sections or transverse (cross) sections, the latter cuts made along the D-V axis. Samples A-C were used to produce sagittal sections, whereas samples D-K were used to produce cross sections. All sections were stained with hematoxylin and eosin (H & E) stain. The H & E stained sagittal and cross sections were imaged with light microscopy. Optical micrographs were taken with an Olympus BX51M microscope in standard and differential interference contrast (DIC) mode. Fig. 3 shows typical micrographs from histology sections. Sagittal sections clearly show the collagen fibrils, which are relatively straight from that imaging direction (Fig. 3a and b). They form a cross-ply arrangement with well-defined angles (Fig. 3b) relative to the A-P axis, which was carefully tracked during all histology and imaging methods. The average fiber angles were measured for each of the three sagittal sections (anterior, mid and posterior locations) by imaging several sites within each of these groups. The cross-helical arrangement of wound collagen fibers exhibited by the s. compactum results in four measurable fiber angles at any location on the fish skin with respect to the A-P axis, a small (< 90°) and large (> 90°) angle (large+small angle=180°) for each of the two types of alternating lamellae of left- and right-handed helically-wound collagen fibers.

2.2. Results

Mean collagen fiber angles (small angles) were calculated at all three A-P locations (anterior, mid and posterior) for both fibers or lamellae in the anteroventral-posterodorsal (AV-PD) and the antero-dorsal-posteroventral (AD-PV) direction, or left and right helices, respectively, for the left side of the fish. Mean AD-PV collagen fiber angles of the s. compactum for anterior, mid and posterior A-P locations were 53.8 ± 1.2 (n=4 sites within inner region of sagittal section), 42.8 ± 0.7 (n=5) and 40.7 ± 2.6 (n=3) °, respectively (Fig. 3c). Mean AV-PD fiber angles for anterior, mid and posterior locations were 58.5 ± 0.9 (n=4), 50.2 ± 1.2 (n=5) and 49.0 ± 2.9 (n=3)°, respectively (Fig. 3c). A pattern of decreasing fiber angle from the head to the tail region of the fish was observed for both AD-PV and AV-PD fibers (Fig. 3c). The collagen fiber angles (and crimp angles described in the next paragraph) reported along the A-P axis of the fish showed similar patterns as in the shark and teleost skin previously studied (Wainwright et al., 1978; Naresh et al., 1997; Hebrank and Hebrank, 1986; Motta, 1977). At all three A-P locations, AV-PD fibers

Fig. 3. Optical micrographs of H & E stained sagittal sections of striped bass skin in both (a) standard and (b) DIC modes, showing the s. compactum and its crossed arrangement of collagen fibers, including fiber angle measurements; (c) diagram of the cross-helical arrangement of collagen fibers of the s. compactum in striped bass fish skin, showing measured fiber angles with respect to the anteroposterior axis (small, < 90°) at three locations (anterior, mid, posterior) and for both left and right helices (blue and red lines, respectively); (d) optical micrograph (with enlarged portion) of an H & E stained cross section of striped bass skin, showing the s. compactum and the crimping of collagen fibers, which can be characterized by crimp amplitude A and wavelength l_O; (e) values for straightening strain ε_s of collagen fibers calculated at different locations, based on A and l_O. (For interpretation of the references to color in this figure legend, the reader is referred to the web version of this article.)

exhibited a higher fiber angle than AD-PV fibers (Fig. 3c).

Even though the fibers are almost continuous within the tissue, the fibers shown in Fig. 3a,b appear to be discontinuous. This effect arises because the fibers are not straight in the out-of-plane (sagittal or along the fiber) direction, but instead are significantly wavy or "crimped", and because some of these fibers were cut during the specimen preparation steps. Fig. 3d shows the cross section of the tissue, where the multi-layered structure of the fibers is evident. In addition to winding about the axis of the fish in a cross helical manner, the fibers are also substantially crimped at a smaller length scale, a particular morphology which can be conveniently fitted with a function of the form $f(x) = A\sin(\pi x/l_o)$, where A is the crimp amplitude and l_o is the crimp wavelength (Wainwright et al., 1976; Hansen et al., 2002). The contour length of the fiber over one wavelength can then be approximated as $L = \pi[1.5(l_o/2 + A) - (Al_o/2)^{0.5}]$. Typically, stretching of this type of tissue is initially dominated by un-crimping, or straightening of the fibers, which only requires a small amount of stress (Wainwright et al., 1976; Hansen et al., 2002; Sherman et al., 2015). Once the fibers are straightened, they start carrying the tensile stress directly, at which point the tissue stiffens significantly. Because the onset of stiffening is governed by the un-crimping of the fibers, the strain at stiffening (or straightening strain), ε_s, can be predicted from the wavelength and amplitude of the crimps (Wainwright et al., 1976; Hansen et al., 2002; Sherman et al., 2015). By considering a section of fibers of length L and initially crimped with a wavelength l_o, the strain at stiffening, corresponding to the strain at which the fibers straighten from the crimped configuration, can be written as $\varepsilon_s = (L - 2l_o)/2l_o$. For each of the eight cross sections (anterior, mid and posterior locations), several sites within the inner undamaged region of the section were imaged to produce an average ε_s for each of three A-P locations. Mean ε_s of collagen fibers of the s. compactum for anterior, mid and posterior locations were 31.1 ± 4.8 ($n=4$), 25.3 ± 1.5 ($n=7$) and 24.5 ± 1.8 ($n=3$) %, respectively (Fig. 3e). A pattern of decreasing ε_s of collagen fibers from the head to the tail region of the fish was observed (Fig. 3e).
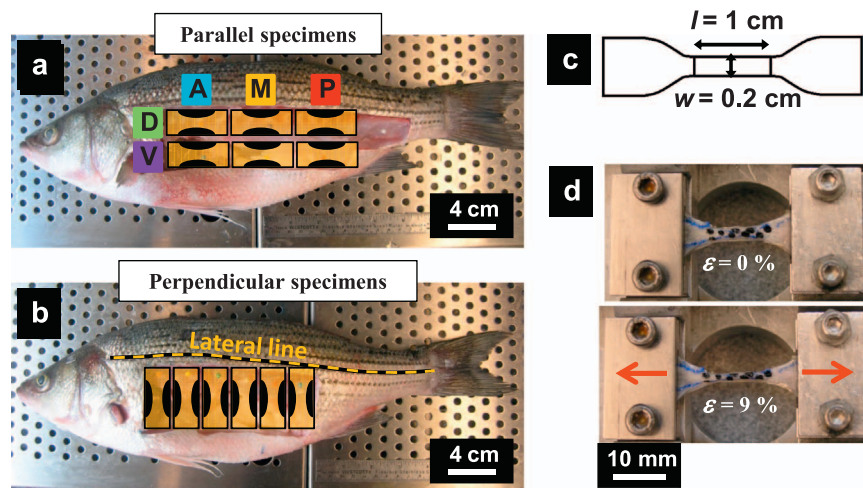
3. Tensile response of s. compactum

3.1. Experimental setup

The dissection procedure for tensile tests on fish skin started with rinsing the fish with cold water for several minutes and descaling one side of the fish from the lateral line down to the ventrum. The descaled region of the fish was patted dry and lines were drawn with a marker to outline either six parallel (anteroposterior, A-P) specimens or six perpendicular (dorsoventral, D-V) specimens, as indicated in Fig. 4a and b. Three parallel specimens were located immediately below the lateral line and the other three parallel specimens were located immediately ventral to the upper three specimens (Fig. 4a). The rectangular-shaped areas ($l \times w = 5 \times 2$ cm) outlined with the marker for either parallel or perpendicular specimens were carved out using a scalpel. The tissue block was immediately dissected to isolate the s. compactum layer and overlying epidermis from the hypodermis and musculature. The prepared specimens were patted dry, sealed in labeled plastic bags, and placed in a freezer at −20 °C for preservation until tensile tests were performed. Prior to testing, the skin samples, still in plastic bags, were thawed in room temperature (~20 °C) water for approximately 30 min. The skin specimens were then removed from the sealed bags and submerged in room temperature water for at least 15 min before tests to completely thaw and rehydrate the samples. In order to test for possible effects of freezing and thawing on specimen mechanical properties, tensile tests were performed on control samples in the fresh state (immediately after dissection), and no significant differences were observed between the tensile properties of fresh versus frozen and thawed specimens.

Using a Teflon sheet, a dumbbell-shaped stencil was constructed to precisely cut specimens for tensile tests on fish skin (Fig. 4c). The dumbbell-shaped skin specimens had a gauge length and width of 1 cm and 0.2 cm, respectively (Fig. 4c). The thickness of the gauge region was measured for each specimen using digital calipers. The mean gauge thickness for all specimens ($n=69$) was $0.234 \pm 2.28 \cdot 10^{-3}$ mm. A speckle pattern of marker dots was applied to the inner (s. compactum) surface of the specimen to measure strains from images acquired during the test (Fig. 4d). The skin specimens were then mounted on a miniature loading stage (Ernest F. Fullam Inc., Latham, NY, USA) with the embedded portion of the specimen well-secured within the clamps using abrasive paper to prevent slippage from the grips. The specimens were pre-loaded with a small force (0.1 N) at a low extension rate to remove any slack before load and extension values were zeroed. The specimens were then stretched at a rate of 0.005 mm s^{-1} (corresponding to a strain rate of ~5.0×10^{-4} s^{-1}) until complete failure, which occurred in the gauge region for all samples. Images were taken throughout the test every 0.5 mm extension and at a higher frequency towards the end of the test to obtain an image of the specimen immediately before failure. Special care was taken to keep the specimens hydrated throughout the preparation steps, during the mounting procedure and during the tests.

For all tensile test specimens (parallel and perpendicular at all anatomical locations), the stress (σ, MPa) was calculated as force/

Fig. 4. Locations and orientations of the samples used for tensile tests on fish skin including (a) parallel (anteroposterior, A-P) and (b) perpendicular (dorsoventral, D-V) orientations and at different locations on the fish (D or V for parallel specimens, and A, M and P locations for all specimens); (c) diagram of the tensile test specimens (adapted from ASTM-D412); (d) typical fish skin tensile test specimen at zero and maximum strain.

initial cross-sectional area, where cross-sectional area was computed as the product of the width and thickness of the gauge region of the specimen. Image analysis and strain measurements were performed using ImageJ Version 1.46r. At high magnification, the gauge region of the specimen at zero strain (first image) was examined. Two distinct ink dots from the speckle pattern were selected at both ends of the gauge region and along its midline. A line was drawn connecting the two marks and the length of the line measured in pixels. The final image of the specimen (immediately prior to failure), was also examined at high magnification. The same two ink dots were located, a line drawn to connect the marks, and the length measured in pixels. The strain of the gauge region was then calculated as change in length (pixels) / initial length (pixels).

3.2. Results

The resulting stress-strain curves from tensile tests on parallel (A-P directed) specimens are shown in Fig. 5. Parallel specimens were prepared from three different fish ($N=3$), with $n=11$, $n=10$, and $n=12$ skin specimens dissected from the three fish (all data plotted in Fig. 5). As expected for tissues made of crimped fibers, the tissues are initially soft, and stiffen at larger strains as the fibers straighten and align along the direction of loading (Fig. 5). The three fish samples all exhibited a similar range of stress-strain curves, failing at stresses in the 20–60 MPa range and at strains in the 0.2–0.5 range. However, marked differences were observed when the stress-strain results were examined for possible A-P and D-V location effects. Parallel specimens from the posterior region exhibited notably stiffer and stronger tensile responses compared to specimens from the anterior region, while mid-region specimens displayed intermediate results (Fig. 5a). Similarly, a strong effect of D-V location was also observed, with dorsal specimens displaying stiffer and stronger responses (Fig. 5b).
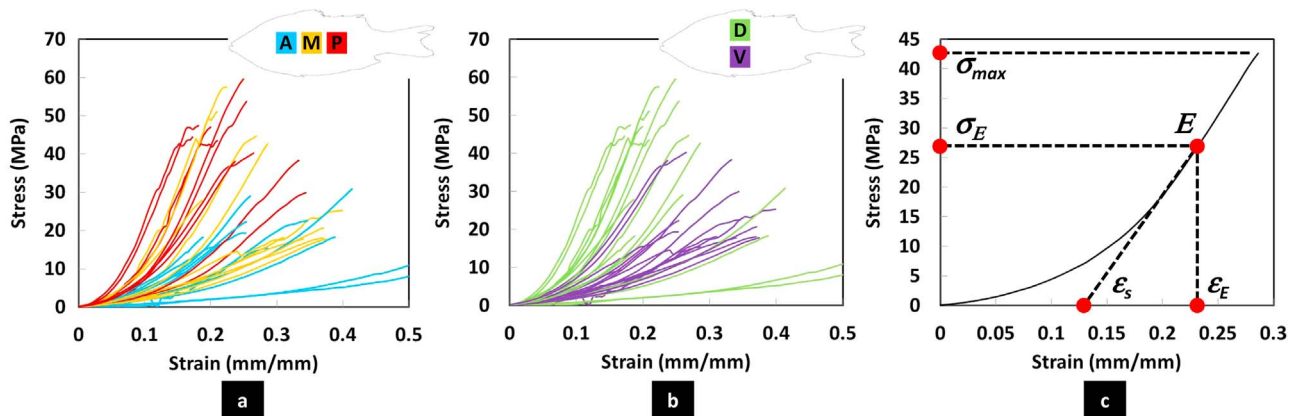
Several material properties were calculated from these stress-strain curves (Fig. 5c). The tangent modulus was computed as the slope of the stress-strain curve. The tangent modulus was initially low for all curves and increased to a maximum value as the fiber angle decreased. Following this stage, the tangent modulus decreased slightly, an indication of damage in the overextended tissue. The modulus for each specimen (E, MPa) was taken as the maximum value of the tangent modulus. The point of maximum tangent modulus was located on the stress-strain curve, and the tangential line at that point was extended to intersect the horizontal axis, thus defining a strain value which we took as the strain at stiffening (ε_s, mm/mm). ε_s was directly obtained by the equation, $\varepsilon_s=(-\sigma_E/E)+\varepsilon_E$, where ($\varepsilon_E$, σ_E) are the coordinates of the point of maximum tangent modulus and E the tangent modulus at that point (i.e. the modulus of the material). Finally, the strength of the

tissue was simply taken as the maximum stress, σ_{max}. The effects of A-P and D-V location on the σ_{max}, E and ε_s of parallel specimens are shown in Fig. 6.

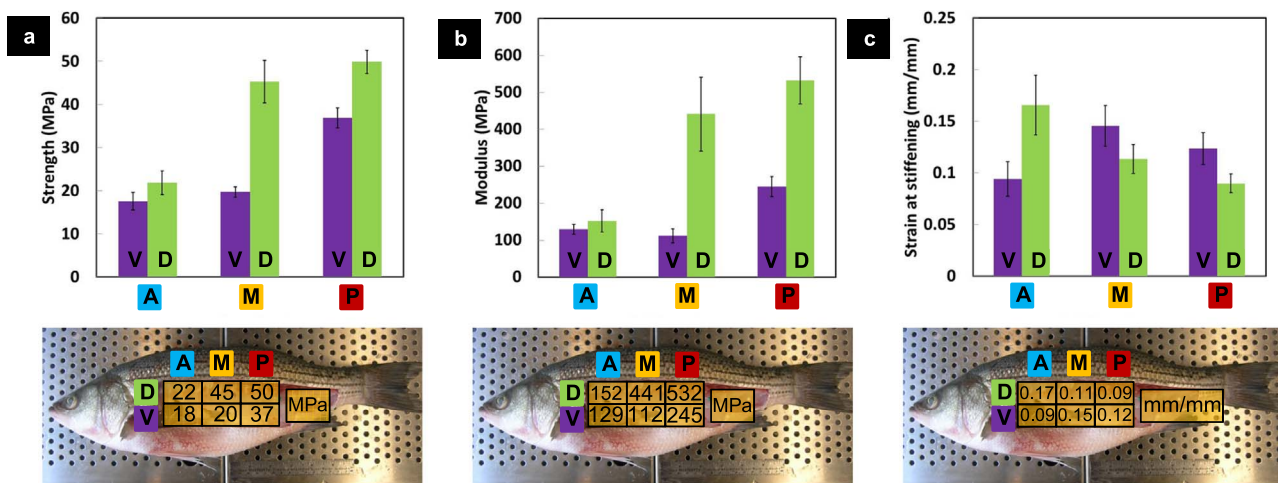Strong positive linear correlations were found between σ_{max} and A-P location for both dorsal ($R=0.81$) and ventral ($R=0.80$) specimens, with dorsal specimens displaying uniformly stronger responses compared to ventral specimens (Fig. 6a). Similarly, strong positive correlations were determined between E and A-P location for both dorsal ($R=0.73$) and ventral ($R=0.61$) specimens, with dorsal specimens showing increased E values (Fig. 6b). A strong negative correlation ($R=0.66$) was found between ε_s and A-P location for dorsal specimens (Fig. 6c). A weak positive correlation ($R=0.30$) was found between ε_s and A-P location for ventral specimens. The number of parallel specimens dissected from the anterior, mid and posterior locations of the three fishes were $n=6$, $n=5$ and $n=6$, respectively, for dorsal specimens, and $n=6$, $n=6$ and $n=4$, respectively, for ventral specimens. Standard two-tailed, unpaired two-sample Student's t-tests assuming unequal variances were employed to compare the mean values reported for the tensile tests. The mean σ_{max} and E of posterior specimens were significantly higher than those of anterior specimens for both dorsal and ventral specimen types ($p < 0.05$) (Fig. 6a and b). The mean ε_s of posterodorsal specimens was lower than that of anterodorsal specimens ($p=0.066$) (Fig. 6c). In summary, the skin in the parallel direction was stronger, stiffer and stiffened faster in the posterior regions compared to the anterior region, and this trend was most pronounced in the dorsal region of the fish.

We also tested the effect of orientation on the tensile response of skin specimens. Perpendicular specimens were prepared from three different fish ($N=3$), with $n=12$ skin specimens dissected from each of the three fish (all data plotted in Fig. 7). Clear differences were observed between the stress-strain curves of parallel versus perpendicular specimens, with perpendicular specimens exhibiting notably stiffer and stronger results, and a lower ε_s (Fig. 7a). The mean σ_{max} and E of perpendicular specimens were significantly higher than those of parallel specimens ($p < 0.05$) (Fig. 7c and d), whereas perpendicular specimens exhibited a significantly lower ε_s ($p < 0.05$) (Fig. 7e). No A-P location effects were determined for perpendicular specimens (Fig. 7b), which displayed a narrower range of stress-strain results than parallel specimens (Fig. 7a).

The overall tensile behavior of the s. compactum can therefore be characterized as relatively stiff and strong compared to other collagenous tissues. S. compactum is about 10-50x stiffer and 3-5x stronger than human skin in tension (Wegst and Ashby, 2004). It is slightly stiffer and stronger than human ligament, but not as strong and stiff as human tendon (Wegst and Ashby, 2004). The stiffness and strength of s. compactum are comparable to the tensile properties of striped bass

Fig. 5. (a) Stress-strain curves for tensile tests on striped bass ($N=3$) fish skin in the parallel orientation ($n=33$ specimens) color-coded for anteroposterior (A,M,P) locations; (b) stress-strain curves for parallel specimens coded for dorsoventral (D-V) location; (c) typical tensile stress-strain curve showing maximum tangent modulus E, strength σ_{max}, stress at maximum tangent modulus σ_E, strain at maximum tangent modulus ε_E, and strain at stiffening ε_s. (For interpretation of the references to color in this figure legend, the reader is referred to the web version of this article.)
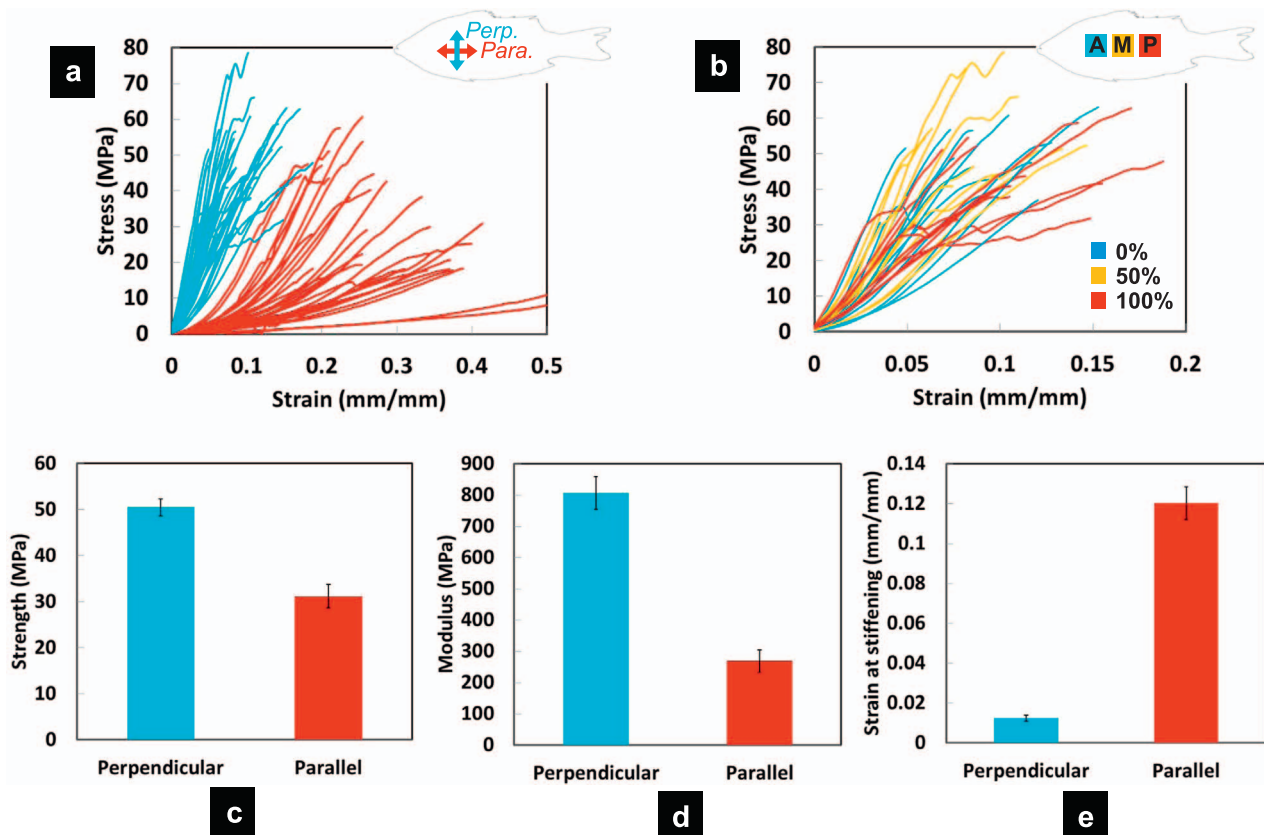
Fig. 6. Summary of results from the tensile tests: mean ± s.e. (a) strength σ_{max}, (b) Modulus E and (c) strain at stiffening ε_s of parallel specimens from all anteroposterior (A-P) and dorsoventral (D-V) locations.

scales (Zhu et al., 2012), which can be explained by their similar composition and arrangement of the collagen fibers into cross-plies. However, as opposed to s. compactum, which displays a soft initial region due to un-crimping of the fibers, the scales show an immediate stiff response because the fibers in that material are straight (Zhu et al., 2012). The s. compactum may therefore contribute to the mechanical protection of the fish, and may also function as an external tendon to enhance swimming efficiency. We further explore these hypothesis in the next two sections.

4. Puncture resistance of s. compactum

Considering the relatively high tensile strength of stratum compactum, there is a clear possibility that this tissue contributes to the mechanical protection of the fish. In this short section we present results on the resistance of the s. compactum against sharp puncture. The experiment consisted of driving a sharp steel needle (tip radius=25 μm) into the skin of a striped bass, with natural muscles and soft tissues as backing material. Details on the setup and procedure for these experiments can be found elsewhere (Zhu et al., 2013). Typical results of puncture tests on scaled and descaled skin from striped bass

Fig. 7. (a) Stress-strain curves for tensile tests on striped bass fish skin in parallel (*N*=3 fish, *n*=33 specimens) and perpendicular (*N*=3 fish, *n*=36 specimens) orientations; (b) stress-strain curves for perpendicular specimens color-coded for anteroposterior (A-P) location; mean ± s.e. (c) strength σ_{max}, (d) modulus E and (e) strain at stiffening ε_s of parallel versus perpendicular specimens. (For interpretation of the references to color in this figure legend, the reader is referred to the web version of this article.)

are shown in Fig. 8. Although the scaled skin exhibited a puncture force about four times greater than that of descaled skin, the descaled skin still displayed a relatively high puncture force of ~2 N. The force required to drive the same needle into the underlying tissues is comparatively negligible, which demonstrates the substantial contribution made by the s. compactum to the puncture resistance of the natural skin. This finding suggests an important mechanical role of the s. compactum, and not just of collective scale mechanisms (Zhu et al., 2013), in increasing the penetration resistance of the skin. The possible function of the s. compactum in improving the penetration resistance of the skin was first proposed for the s. compactum of shark skin (Motta, 1977), but the data reported here clearly demonstrate the contribution of the s. compactum to the puncture performance of teleost skin. This simple experiment supports the idea that one of the functions of stratum compactum is to provide a "last barrier" of protection against puncture and lacerations.

5. Bending tests on whole fish: s. compactum as an external tendon?

5.1. Experimental setup

The objective of this test was to assess the contribution of the s. compactum to the bending stiffness of the whole fish. The underlying question is related to the exotendon hypothesis: If the s. compactum is found to carry a significant portion of the bending loads, especially at high curvatures, then it is likely that it acts as a mechanical energy storage device, contributing to swimming efficiency. This test consists of bending the whole fish with a stiff wire in series with a calibrated spring (Fig. 9a). By increasing the tension in the wire, the fish is bent by different amounts of curvature, and pictures of the whole fish are acquired at each position. The analysis of the images together with the knowledge of the force carried by the spring were used to determine the curvature-bending moment at any cross section in the fish. The dissection procedure and experimental setup employed in this study to perform whole fish bending tests were as follows. The fish were kept on ice before testing and all tests were commenced within a few hours of purchasing the fish specimens. The fish were preconditioned by rinsing with cold water and gently flexing the fish for 5 min before tests to raise the temperature of the fish samples and bring them closer to physiological body conditions (the flexural rigidity of the samples was lower after preconditioning). The fish skin was gently descaled over its entire surface, and the anterior and posterior dorsal fins and the caudal fin of the fish were removed.

About 20 pins were inserted into the body of the fish along the mid-dorsal line and evenly spaced from the tail to the head region (Fig. 9a) in order to track the position of the dorsal line. A hole was made through the tail of the fish below the last pin in order to secure one end of the pulling cable. The operculum in the pharyngeal region of the fish was removed on both sides of the head and a small passage was cleared through the rostrum to secure the other end of the cable. The fish was then placed belly down on an immersible Plexiglas support board with a clamp fixed to one end of the board. The support board and ventral half of the fish were submerged in ice water, and a fish hook was inserted through the hole in the tail. A calibrated tensile spring (stiffness = 0.623 N/mm) was attached at one end to the fish hook, and at the other end to steel wire. The steel wire was fed through the fish's rostrum and connected to the clamp, and the length of the connection could be changed by sliding the wire through the rostrum, thus causing the fish to bend. The clamp was used to secure the wire and set the bending to a fixed position. An Olympus digital camera (model no. C-5060) on a tripod was positioned over the setup in order to take high-resolution images of the fish at each bending position.

The bending tests started with the fish in a straight body position. The wire was then pulled by small (~1 N) increments, and a picture was taken at each bending position (~15 positions per test) until a high

body curvature was achieved. The descaled fish was first tested three times with intact s. compactum (control group), and then tested three times with the s. compactum disrupted. Using a 500 µm control-depth surgical knife ($author1$ et al., Shreeji Micro Systems Inc.), nine vertical incisions were made to the skin on both sides of the fish from the head to the tail region (Fig. 9b). The incisions were ~32 mm in length and had an anteroposterior (A-P) spacing of ~25 mm. The 500 µm control-depth knife allowed precise targeting and disruption of the s. compactum layer of the skin without significant damage to the underlying muscle, because our histology results suggest that the hypodermis, the intervening tissue layer between the s. compactum and underlying muscle, is on average located at a depth of ~500 µm from the skin surface. Some tissue degradation may have occurred before sample collection and thus the flexural properties of the fish and effects of s. compactum disruption were possibly somewhat different than those of living fish with active and stiffer musculature, but as described in the results and discussion, the effect of s. compactum incision is likely similar. Furthermore, in order to test for possible degradation of properties during the course of flexural tests, another "control fish" was tested in bending at the very beginning of the test session, and subjected to the same temperature and hydration as the tested fish. The control fish was tested again at the very end of the session. No change in properties was observed in the control fish, and therefore no significant degradation of properties occurred over the course of the testing session.

The data analysis used in this study to analyze the whole fish bending test data was as follows. Image analysis was performed using the software Plot Digitizer Version 1.9, and the data were processed with Matlab Version R2011b. Within each image, a coordinate system (x,y) was first defined. The x axis coincided with the axis of the spring, i.e. with the line of action of the tensile force carried by the cable, and the origin of the coordinate system was defined as the intersection between the x axis and the dorsal line of the fish (Fig. 9a). The axis y was then chosen to be perpendicular to the x and in the normal direction, to form a coordinate system (x,y). Using this system, the coordinates of the pins (P_1 to P_{20} in Fig. 9a), as well as the coordinates of points S_1 and S_2 located at the ends of the spring, were collected. The process of determining the system (x,y) was repeated for each image because the fish may rotate or translate between each of the loads. A curvilinear coordinate system s was also defined along the dorsal line. For each image, the local curvature of the dorsal line of the fish was measured as a function of curvilinear coordinate s, by fitting a circle onto a segment of the profile of length Δs centered on the point where curvature was calculated. The curvature (mm^{-1}) was computed as the inverse of the radius of the circle. The coordinates S_1 and S_2
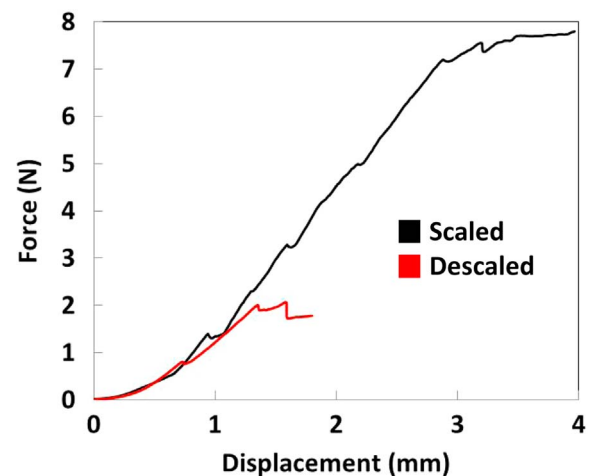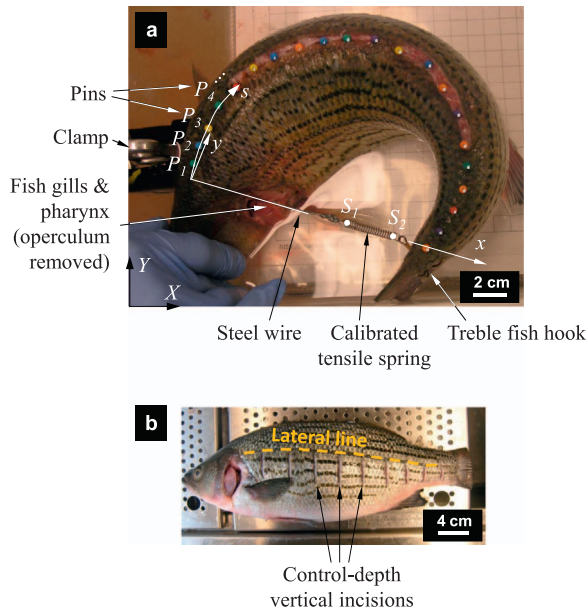

Fig. 8. Representative force-displacement curves for puncture tests on scaled (natural, intact) and descaled striped bass fish skin.

Pins

Clamp

Fish gills &
pharynx
(operculum
removed)

Steel wire   Calibrated   Treble fish hook
              tensile spring

Fig. 9. (a) Experimental setup for bending tests on a whole striped bass and measurements from image analysis; (b) fish specimen used in bending tests showing control-depth incisions made to the s. compactum.

were used to calculate spring extension, which in turn was used to calculate the tensile force in the cable. The bending moment M was then calculated at any point along the fish using the simple formula $M = F \cdot y_C$, where y_C is the vertical coordinate of point C, defining a virtual cross section along the fish (Fig. 10a).
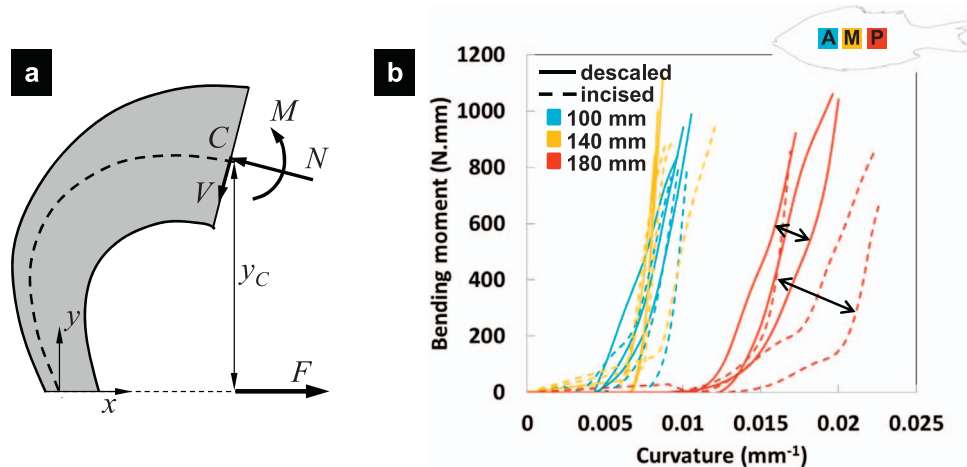
5.2. Results

Fig. 10b shows bending moment-curvature (M-C) curves measured at three locations (s distances) along the mid-dorsal line (A-P axis): 100 mm in the anterior region, 140 mm in the mid-region, and at 180 mm in the posterior region. Although the mid-region of the fish exhibits the stiffest flexural response (lowest curvature at stiffening and highest stiffness), M-C curves display a similar shape at all three A-P regions of the fish. At low curvatures, a soft flexural response is observed, whereas at higher curvatures, significant stiffening occurs. A rightward shift of the M-C curves and decrease in flexural stiffness along the M-C curve was observed at all three A-P locations upon s. compactum incision,

but was more pronounced for the thinner A and P ends of the fish (Fig. 10b). These experiments demonstrate that the s. compactum therefore carries a significant portion of the bending moment.

6. Discussion

The body of observations and measurements on s. compactum gathered here leads to a clearer picture of the structure-properties-function relationships in this material. In tension, s. compactum is stronger, stiffer and stiffens faster in the posterior regions compared to the anterior region, and this trend is the most pronounced in the dorsal region of the fish. In addition, s. compactum is stiffer and stronger in the perpendicular direction compared to the longitudinal (parallel) direction. These trends may be explained by micro-mechanisms associated with the collagen fibers, which dominate the structural and mechanical response of this material. From histology, it was shown that both AV-PD and AD-PV directed fibers of the s. compactum exhibit a pattern of decreased collagen fiber angle towards the tail region, with AV-PD fibers exhibiting higher fiber angles. In addition, it was shown that the strain at stiffening ε_s of collagen fibers also decreases towards the posterior region. Similar results were found by Naresh et al., (1997) for shark skin, that is, they determined patterns of decreased collagen fiber and crimp angle towards the caudal region. As suggested by Naresh et al., (1997) and in support of the original s. compactum exotendon hypothesis (Wainwright et al., 1978), the mechanical properties of the skin, which are dominated by the properties of the s. compactum that composes the majority of the integument, may be controlled primarily by the collagen fiber and crimp angles of the s. compactum. These two variables, along with elastin content, were proposed by Naresh et al., (1997) to be the strongest factors influencing the measured tensile properties of the skin, including the observed specimen location and orientation effects.

Our results for striped bass also suggest that the tensile performance of the skin is determined by A-P and D-V location and thus by local histological features that vary along these axes, including collagen fiber angle and ε_s of collagen fibers. The lower tensile ε_s of parallel specimens from the posterodorsal region compared to the anterodorsal region may be explained by the lower collagen fiber angle and ε_s of collagen fibers measured for this area of the skin, as the fibers would be expected to align with the axis of force and become less crimped at a lower strain, thus resulting in earlier stiffening. The higher E and σ_{max} of both dorsal and ventral specimens from the posterior region compared to the anterior region may be explained by recruitment of collagen fibers. That is, a higher total number of collagen fibers may be

Fig. 10. (a) Free body diagram of the bent fish. Shown are variables: C (location of virtual cross section), V (shear force), M (bending moment), N (normal force), y_C (distance from x axis to point C), F (force acting on the spring); (b) Bending moment-curvature (M-C) curves at three locations along the mid-dorsal line (anteroposterior, A-P, axis): 100 mm in the anterior region, 140 mm in the mid-region and 180 mm in the posterior region, for a striped bass fish in both "descaled" and s. compactum "incised" conditions, (black arrows indicate the rightward shift of M-C curves at 180 mm after s. compactum incision).

recruited and align with the axis of force before failure of the fibers that were first aligned occurs (assuming all fibers do not align uniformly), which would result in higher E and σ_{max} due to a greater number of collagen fibers being loaded before failure. Similarly, the lower ε_s of perpendicular specimens versus parallel specimens may be explained by their lower fiber angles relative to the axis of force, and the higher E and σ_{max} values by increased recruitment of collagen fibers before failure.

In addition, although the tensile ε_s of parallel specimens and the ε_s of collagen fibers from histology both displayed the predicted trend of decreased ε_s towards the posterior region of the fish, it was observed that the tensile ε_s values were notably lower than the corresponding collagen fiber ε_s values. The tensile ε_s of parallel specimens ranged from 17% in the anterodorsal region to 9% in the posterodorsal region, whereas the ε_s of collagen fibers ranged from 31% in the anterior region to 24% in the posterior region. However, the mean ε_E of parallel specimens ranged from 29% in the anterodorsal region to 15% in the posterodorsal region, which are closer in magnitude to the ε_s of collagen fibers from histology. This finding suggests that the significant stiffening observed near the end of the stress-strain curve is, as predicted, a result of un-crimping of collagen fibers in conjunction with alignment of the fibers along the axis of force. Therefore, the anisotropic (direction-dependent) tensile properties of striped bass fish skin from different anatomical locations are explained well by local structural features of the s. compactum, including collagen fiber angle and ε_s.

This structure and mechanical response is adapted to the function of the s. compactum. In particular, we showed s. compactum by itself can provide an appreciable barrier to sharp puncture. As well, the tensile properties of the skin and s. compactum in the A-P direction are most physiologically relevant to fish locomotion as this is the natural direction of stretching on the convex side of the fish during swimming. Regardless of A-P location, the collagen fiber angle of the s. compactum always exceeds 45° and the lamellae always exhibit a degree of crimping, and thus these structural attributes generate an initial compliant tensile response followed by significant stiffening, with the E, σ_{max} and ε_s dependent on the local collagen fiber angle and ε_s. These tensile properties are necessary for the s. compactum of striped bass skin to function as an exotendon at a late stage in the locomotory cycle, and support the s. compactum exotendon hypothesis for striped bass skin, which was further explored using whole fish bending tests with disruption of the s. compactum.

The examination of the contribution of s. compactum to whole body flexural stiffness was comparable to Long et al. (1996), who investigated the flexural behavior of longnose gar (*Lepisosteus osseus*) and revealed an effect of selective dermal incision and removal of a row of thick, mineralized ganoid scales on the flexural stiffness recorded for this smaller, primitive fish species. The ablation treatments used by Long et al. (1996) caused a rightward shift of the *M-C* curve measured for longnose gar that was similar to the decrease in flexural stiffness observed in this study for striped bass after incision to the s. compactum. For the s. compactum to function as a tendon-like energy storage device and assist with fish locomotion, it is necessary that it stores and releases sufficient strain energy to facilitate muscle contraction. This energy storage and recovery capability was supported for the s. compactum of striped bass by the reduction in body flexural stiffness after s. compactum incision, which would likely also result in decreased energy absorbed at maximum curvature of the fish. It is also necessary that the energy is stored and recovered at the correct stages in the fish locomotory cycle, which highlights the importance of the "neutral zone" (Long et al., 1996), or initial compliant response of the fish upon flexure before stiffening occurs at high body curvatures.

The shape of stress-strain curves from tensile tests on descaled fish skin in the A-P direction closely resembles that of *M-C* curves from whole fish bending tests, during which the fish exhibits an initial compliant flexural response followed by significant stiffening, and both

stress-strain and *M-C* curves resemble the stress-strain curve of mammalian tendon (Wainwright et al., 1976). Although the tensile behavior of the s. compactum as part of the intact integument during fish locomotion may differ somewhat from that of isolated skin specimens tested in tension along the A-P axis, the tensile response observed for such isolated samples conformed to the general hypothesis of s. compactum exotendon function, which requires an initial compliant phase permitted via shearing of lamellae (and alignment of collagen fibers) and un-crimping of collagen fibers as described by Wainwright et al. (1978), Whitear (1986), Naresh et al. (1997), Elliot (2000) and Hebrank and Hebrank (1986), followed by marked strain hardening or stiffening from collagen fiber recruitment that allows sufficient energy absorption and recovery to assist with the subsequent stage of locomotion. During fish swimming, the s. compactum would operate in a similar manner on the convex side of the fish allowing for the initial compliant phase or "neutral zone" (Long et al., 1996) observed for *M-C* curves from whole fish bending tests and producing an initial low flexural stiffness. The stiffening observed near the end of *M-C* curves was suspected to arise in part from the s. compactum if the skin is indeed functioning as an external tendon. The contribution of the s. compactum to flexural stiffness of the fish at high strains or body curvatures was demonstrated from the incision experiments, which inhibited s. compactum function and resulted in decreased stiffness and likely energy absorption, thus supporting the exotendon hypothesis.

7. Conclusions

The mechanical interaction of teleost fish scales plays an important role in the puncture resistance of fish skin by distributing the force upon puncture and protecting soft underlying tissues. However, the scales contribute a negligible amount of body flexural stiffness and therefore do not function in whole fish swimming mechanics by acting as an external tendon during locomotion. The relatively weak mechanical interaction of scales at high body curvatures and thus negligible contribution to flexural stiffness of the fish is a possible adaption for the enhanced speed and flexibility of modern teleost fish. Instead, the s. compactum layer may provide the skin with tendon-like properties that enhance locomotion. The tensile response of fish skin stretched in anteroposterior direction is generated by two main histological features and mechanisms of the s. compactum, the angle of fibers composing the collagen cross-ply and the crimping of collagen fibers. These structural characteristics of the s. compactum produce the tendon-like response of the skin, including an initial compliant phase and a subsequent stiffening phase that may result in the storage and recovery of elastic strain energy, thus promoting muscular contraction and providing the skin with an external tendon function. The structural and tensile properties of the s. compactum vary across the anteroposterior axis of the fish, with the skin in the dorsal and tail regions displaying the stiffest and strongest responses, suggesting possible differences in function for the different regions of the fish. The s. compactum also increases the flexural stiffness of the fish, which further supports a tendon-like, energy storage device role of this layer of the skin. As well, the s. compactum accounts for a large portion of the puncture resistance of the intact scaled skin, which suggests an additional role of the s. compactum of teleosts in the mechanical protection against predator bites. The structural and mechanical properties of the s. compactum of striped bass skin, in conjunction with research on the puncture and bending mechanics of the scaled skin, could be used in the biomimetic design of artificial materials and systems inspired from teleost fish skin that replicate the range of desirable properties exhibited by this high-performance natural material, including light weight, flexibility, high protective capacity (or puncture resistance), and energy storage and recovery capability (or tendon-like properties).

Acknowledgments

References

ASTM-D412, Standard Test Methods for Vulcanized Rubber and Thermoplastic Elastomers – Tension. Figure 1: Standard Dies for Cutting Dumbbell Specimens.

Bruet, B.J.F., Song, J.H., Boyce, M.C., Ortiz, C., 2008. Materials design principles of ancient fish armour. Nat. Mater. 7, 748–756.

Dastjerdi, A.K., Barthelat, F., 2015. Teleost fish scales amongst the toughest collagenous materials. J. Mech. Behav. Biomed. Mater. 52, 95–107.

Elliot, D.G., 2000. Chapter 5 – integumentary system (gross functional anatomy), Chapter 17 – integumentary system (microscopic functional anatomy. In: Ostrander, G.K. (Ed.), The Laboratory Fish. Academic Press, Oxford, 95–108, (271–306).

Hansen, K.A., Weiss, J.A., Barton, J.K., 2002. Recruitment of tendon crimp with applied tensile strain. J. Biomech. Eng. 124, 72–77.

Hebrank, M.R., Hebrank, J.H., 1986. The mechanics of fish skin: lack of an "external tendon" role in two teleosts. Biol. Bull. 171, 236–247.

ImageJ Version 1.46r. ⟨http://rsb.info.nih.gov/ij/⟩.

Long, J.H., Hale, M.E., McHenry, M.J., Westneat, M.W., 1996. Functions of fish skin: flexural stiffness and steady swimming of longnose gar, *Lepisosteus osseus*. J. Exp. Biol. 199, 2139–2151.

Matlab Version R 2011b. ⟨http://www.mathworks.com/⟩.

Meyers, M.A., Lin, Y.S., Olevsky, E.A., Chen, P.-Y., 2012. Battle in the Amazon: Arapaima versus Piranha. Adv. Eng. Mater. 14, B279–B288.

Motta, P.J., 1977. Anatomy and functional morphology of dermal collagen fibers in sharks. Copeia 3, 454–464.

Naresh, M.D., Arumugam, V., Sanjeevi, R., 1997. Mechanical behaviour of shark skin. J. Biosci. 22, 431–437.

Plot Digitizer Version 1.9. ⟨http://plotdigitizer.sourceforge.net/⟩.

Sherman, V.R., Yang, W., Meyers, M.A., 2015. The materials science of collagen. J. Mech. Behav. Biomed. Mater. 52, 22–50.

Shreeji Micro Systems Inc., Gujarat, India. ⟨www.ophthalmicsurgicalblade.com/⟩.

Vernerey, F.J., Barthelat, F., 2010. On the mechanics of fishscale structures. Int. J. Solids Struct. 47, 2268–2275.

Wainwright, S.A., Vosburgh, F., Hebrank, J.H., 1978. Shark skin: function in locomotion. Science 202, 747–749.

Wainwright, S.A., Biggs, W.D., Currey, J.D., Gosline, J.M., 1976. Mechanical Design in Organisms. Edward Arnold Publishers Ltd., London.

Wegst, U.G.K., Ashby, M.F., 2004. The mechanical efficiency of natural materials. Philos. Mag. 84, 2167–2181.

Whitear, M., 1986. The skin of fishes including cyclostomes. In: Bereiter-Hahn, J., Matoltsy, A., Richards, K. (Eds.), Biology of the Integument – 2 Vertebrates. Springer-Verlag, Berlin, 8–77.

Yang, W., Chen, I.H., Gludovatz, B., Zimmermann, E.A., Ritchie, R.O., Meyers, M.A., 2013. Natural flexible dermal armor. Adv. Mater. 25, 31–48.

Zhu, D., Szewciw, L., Vernerey, F., Barthelat, F., 2013. Puncture resistance of the scaled skin from striped bass: collective mechanisms and inspiration for new flexible armor designs. J. Mech. Behav. Biomed. Mater. 24, 30–40.

Zhu, D., Fuentes-Ortega, C., Motamedi, R., Szewciw, L., Vernerey, F., Barthelat, F., 2012. Structure and mechanical performance of a "modern" fish scale. Adv. Eng. Mater. 14, B185–B194.